Inorganic Chemistry

pubs.acs.org/IC Article

Iron(II/III) Halide Complexes Promote the Interconversion of Nitric Oxide and S-Nitrosothiols through Reversible Fe-S Interaction

Anna L. Poptic and Shiyu Zhang*



Cite This: Inorg. Chem. 2021, 60, 5190-5197



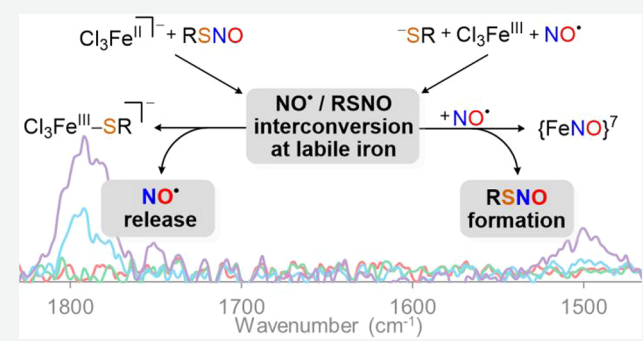
ACCESS

Metrics & More

Article Recommendations

Supporting Information

ABSTRACT: Heme and non-heme iron in biology mediate the storage/release of NO[•] from S-nitrosothiols as a means to control the biological concentration of NO[•]. Despite their importance in many physiological processes, the mechanisms of N–S bond formation/cleavage at Fe centers have been controversial. Herein, we report the interconversion of NO[•] and S-nitrosothiols mediated by Fe^{II}/Fe^{III} chloride complexes. The reaction of 2 equiv of S-nitrosothiol (Ph₃CSNO) with [Cl₆Fe^{II}₂]²⁻ results in facile release of NO[•] and formation of iron(III) halothiolate. Detailed spectroscopic studies, including in situ UV–vis, IR, and Mössbauer spectroscopy, support the interaction of the S atom with the Fe^{II} center. This is in contrast to the proposed mechanism of NO[•] release from the well-



studied "red product" κ^1 -N bound S-nitrosothiol Fe^{II} complex, $[(CN)_5 Fe(\kappa^1-N-RSNO)]^{3-}$. Additionally, Fe^{III} chloride can mediate NO $^{\bullet}$ storage through the formation of S-nitrosothiols. Treatment of iron(III) halothiolate with 2 equiv of NO $^{\bullet}$ regenerates Ph₃CSNO with the Fe^{II} source trapped as the S = 3/2 {FeNO} 7 species $[Cl_3FeNO]^-$, which is inert toward further coordination and activation of S-nitrosothiols. Our work demonstrates how labile iron can mediate the interconversion of NO $^{\bullet}$ /thiolate and S-nitrosothiol, which has important implications toward how Nature manages the biological concentration of free NO $^{\bullet}$.

■ INTRODUCTION

Nitric oxide (NO•) is a crucial secondary signaling molecule responsible for the regulation of a range of biological processes, including immune response, smooth muscle relaxation, and neurotransmission.¹ However, NO• has a short lifetime *in vivo* and quickly reacts with the bioavailable oxygen and superoxide, forming reactive oxygen and reactive nitrogen species.² To mitigate the formation of these reactive species, Nature has developed specific regulatory strategies that store NO• as airstable S-nitrosothiols (RSNOs).³ RSNOs can also serve as signaling molecules to participate in the S-nitrosation of proteins, which is a precisely regulated post-translational modification. Dysregulation of RSNO homeostasis has been linked to several diseases, such as Alzheimer's disease and Parkinson's disease, cancer, diabetes, etc.^{4,5}

Formation of S-nitrosothiols from free NO• and thiol requires one-electron oxidation, which can be facilitated by the single-electron accepting abilities of Fe^{III} or Cu^{II}. Conversely, Fe^{II} and Cu^I can act as one-electron reducing agents to promote the release of NO• from S-nitrosothiols via cleavage of the S-N bond. Several biological iron centers have been implicated in RSNO decomposition/formation. For example, heme-iron proteins, such as cytochrome c, are responsible for the coupling of NO• and low-mass thiols to RSNOs, i.e., S-nitrosoglutathione (GSNO) or S-nitroso-L-cysteine (CysSNO). In addition to enzymatic heme-iron centers, exposure of NO• to intracellular labile iron has been

associated with increased levels of protein S-nitrosation with simultaneous formation of dinitrosyl iron complexes (DNICs). Moreover, the release of NO $^{\bullet}$ from the blood pressure medication sodium nitroprusside (SNP) [Na]₂[Fe-(CN)₅(NO)] is thought to proceed through the decomposition of an iron(II) S-nitrosothiol adduct, [Fe(CN)₅(κ ¹-N-RSNO)]³⁻, known as the "red product". ^{12,13}

Despite the importance of iron centers in facilitating the formation/decomposition of S-nitrosothiols, the discrete molecular mechanisms of N–S bond formation/cleavage at iron sites remain controversial. For example, two mechanisms have been proposed for S-nitrosothiol formation at heme-iron sites. The first involves nucleophilic attack of an iron nitrosyl {FeNO}⁶ species by a thiolate (Scheme 1, top), whereas the second invokes an Fe^{III}—thiolate intermediate undergoing further reaction with free NO[•] (Scheme 1, bottom). Despite the structural characterization of S-nitrosated hemeiron proteins, spectroscopic support for both mechanisms exists. Second invokes an second invokes and second invokes are second invokes and second invokes and second invokes and second invokes are second invokes and second invokes and second invokes are second invokes and second invokes and second invokes are second invokes and second invokes and second invokes are second invokes and second invokes and second invokes are second invokes.

Received: January 21, 2021 Published: March 11, 2021





Scheme 1

$$\begin{array}{c} NO' \\ \hline \\ Fe^{\parallel} \\ \hline \\ L \\ \hline \\ RS^{-} \\ \hline \\ RSNO + Fe^{\parallel} \\ \hline \\ L \\ \hline \\ RSNO + Fe^{\parallel} \\ \hline \\ RSNO + Fe^{\parallel} \\ \hline \\ L \\ \hline \\ \\ \end{array}$$

Significant research efforts have also been devoted to understanding the binding mode of S-nitrosothiols to Fe centers (κ^1 -N vs κ^1 -S) during NO $^{\bullet}$ release from SNP (Scheme 2). Spectroscopic studies suggest that the "red product"

Scheme 2

Too slow to explain the fast vasodilatory effect of SNP

 $[Fe(CN)_5(\kappa^1\text{-N-RSNO})]^{3-}$ extrudes a thiyl (RS^{\bullet}) radical to form a $[(CN)_5FeNO]^{3-}$ complex $(\{FeNO\}^7)$ which then releases free NO $^{\bullet}$. However, both experimental 8,21,22 and computational 23,24,43,44 studies have demonstrated the thiyl radical (RS^{\bullet}) expulsion process in Scheme 2 should be unfavorable since κ^1 -N coordination of S-nitrosothiols strengthens the S-N bond (Scheme 3). Furthermore, the

Scheme 3

RS-N=0

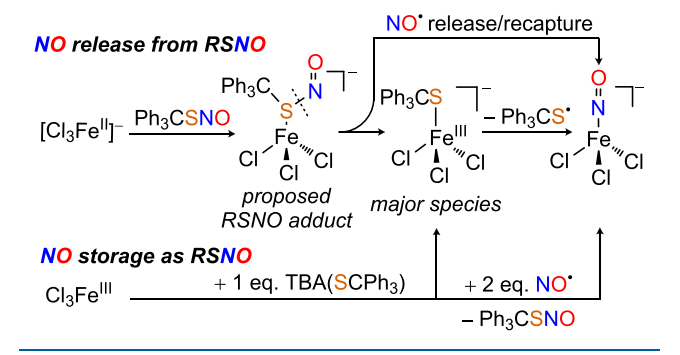
$$\kappa^1$$
-N coordination
 κ^1 -S coordination

currently proposed mechanism does not explain the rapid vasodilatory effect of SNP, given the slow rate of NO• liberation from the $\{\text{FeNO}\}^7$ $[(\text{CN})_5\text{FeNO}]^{3-}$ $(k = 5.0 \times 10^{-5} \text{ s}^{-1}, \text{ Scheme 2}).^{25}$

As the debate for the mechanisms of S-nitrosothiol formation and decomposition at iron sites continues, the mechanism of RSNO formation mediated by the labile iron pool (LIP) also remains ambiguous. Iron within the LIP is present in both Fe^{II}/Fe^{III} oxidation states and can be coordinated by various weak field ligands to form high-spin Fe^{II}/Fe^{III} complexes. $^{10,26-29}$ While Kim and Lippard have investigated the reactivity of NO^{\bullet} with synthetic iron-sulfur clusters $^{30-33}$ and iron(II) thiolates, $^{34-37}$ other simple Fe^{II}/Fe^{III} coordination complexes relevant to the LIP and NO^{\bullet}/S -nitrosothiol interconversion still warrant continued investigation.

Herein, we employ Fe^{II}/Fe^{III} chloride complexes as simplified models for LIP to investigate the potential roles of Fe^{II}/Fe^{III} in RSNO formation/decomposition. We demonstrate that reaction of RSNO with Fe^{II} chloride complexes leads to the facile release of NO[•] from RSNO (Scheme 4). Spectroscopic studies suggest that the Fe^{II} center interacts with the S atom before its conversion to iron(III)—halothiolate and

Scheme 4



NO•. The NO• release from RSNO is reversible, and in the presence of an additional equivalent of NO•, the iron(III)—halothiolate captures NO• to afford RSNO. The Fe^{II} chloride byproduct is trapped by a second equivalent of NO• to form stable {FeNO}⁷ complexes that are inert toward catalytic decomposition of RSNO. This unique property of high-spin iron complexes may be a strategy Nature employs to reversibly regulate the bio-availability of free nitric oxide.

■ RESULTS AND DISCUSSION

Reactivity of Fe^{II} Chloride with S-Nitrosothiols. We began our investigation by preparing an iron(II) halide complex soluble in aprotic solvents. Treatment of PPNCl (PPN = bis(triphenylphosphine)iminium) with anhydrous Fe^{II}Cl₂ in acetone affords PPN₂[Cl₆Fe^{II}₂]. The spectroscopic characterizations of the PPN₂[Cl₆Fe^{II}₂] complex match those reported in the literature.³⁸ The analogous TBA salt of iron(II) trichloride was isolated as colorless crystals by the addition of TBACl (TBA = tetrabutylammonium) to anhydrous Fe^{II}Cl₂. Single-crystal X-ray diffraction analysis indicates that the Fe^{II} centers exist in two types of coordination environments, as $[Cl_6Fe^{II}_2]^{2-}$ and monomeric $[Cl_3Fe^{II}(H_2O)]^{-}$ (Figure S29). The aqua ligand could be a result of H₂O in either TBACl or Fe^{II}Cl₂. Next, we monitored the reaction of [Cl₆Fe^{II}₂]²⁻ with Snitrosotriphenylmethanethiol (Ph₃CSNO) with UV-vis spectroscopy at low temperature. The structural difference between the PPN and TBA salts of the Fe^{II} chlorides in the solid state does not impact their reactivity with S-nitrosothiols (Figures S8, S9). Addition of 2 equiv of Ph₃CSNO to $[Cl_6Fe^{II}_2]^{2-}$ in a 1:1 mixture of THF and CH₃CN at -50 °C affords a dark brown complex with UV-vis absorption bands at 520 nm (ε = 1000 M⁻¹ cm⁻¹) and 630 nm ($\varepsilon = 970 \text{ M}^{-1} \text{ cm}^{-1}$) (Figure 1, brown trace), which slowly converts to a green species at room temperature with absorbances at 365 nm (ε = 1080 M⁻¹ cm⁻¹), 480 nm (ε = 410 M⁻¹ cm⁻¹), and 660 nm (ε = 320 M⁻¹ cm⁻¹) (Figure 1, green trace). The final green complex was identified as S = 3/2 TBA[Cl₃FeNO], which can be independently synthesized by treatment of $[Cl_6Fe^{II}_2]^{2-}$ with NO (Figures S1, S4). 39 On the basis of the absorptivity of [Cl₃FeNO]⁻, the yield of TBA[Cl₃FeNO] was approximately quantitative. The [Cl₃FeNO]⁻ anion was observed first by Kohlschütter⁴⁰ and structurally characterized by van Eldik,⁴¹ Beck, 42 and Klüfers. 39 The S = 3/2 spin state of $[Cl_3FeNO]^$ was established recently based on SQUID measurement³⁹ and our Evans method study (see Supporting Information (SI)). The [Cl₃FeNO]⁻ complex is remarkably stable to oxygen and moisture, and no decomposition of PPN[Cl₃FeNO] solid was observed even after storage under ambient conditions for several days.

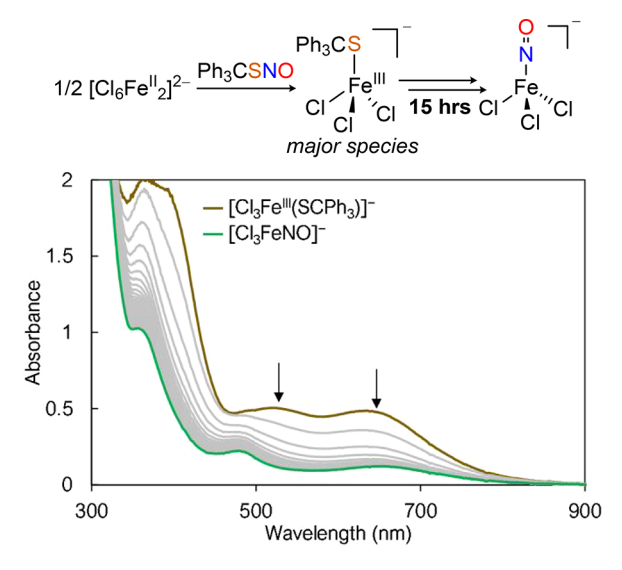
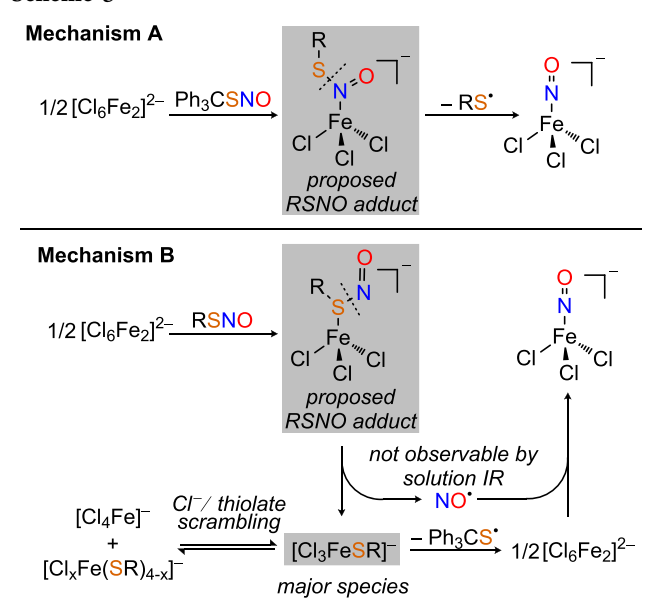


Figure 1. In situ UV—vis spectra of the treatment of $[Fe_2Cl_6]^{2-}$ with 2 equiv of Ph₃CSNO at -50 °C in 1:1 THF/CH₃CN (0.5 mM). The brown intermediate $[Cl_3Fe(SCPh_3)]^-$ ($\lambda_{max1}=520$ nm ($\varepsilon=1000$ M $^{-1}$ cm $^{-1}$), $\lambda_{max2}=630$ nm ($\varepsilon=970$ M $^{-1}$ cm $^{-1}$)) was converted after 15 h (scan rate 30 min) to $[Cl_3FeNO]^-$ (green trace) ($\lambda_{max1}=365$ nm ($\varepsilon=1080$ M $^{-1}$ cm $^{-1}$), $\lambda_{max2}=480$ nm ($\varepsilon=410$ M $^{-1}$ cm $^{-1}$), $\lambda_{max3}=660$ nm ($\varepsilon=320$ M $^{-1}$ cm $^{-1}$).

Scheme 5



Two possible mechanisms could explain the formation of $[Cl_3FeNO]^-$ (Scheme 5). On the basis of the proposed mechanism of NO erelease from SNP (Scheme 2), one could envision coordination of Ph_3CSNO to the Fe^{II} center to form an Fe^{II} κ^1 -N S-nitrosothiol adduct, followed by thiyl radical extrusion to afford $[Cl_3FeNO]^-$ (Mechanism A, Scheme 5, top). However, Mechanism A contradicts the chemical reactivity of metal S-nitrosothiols described in Scheme 3. 8,21,22 Therefore, an alternative mechanism in which the Fe^{II} center interacts with the S atom warrants consideration (Mechanism B, Scheme 5, bottom). In this case, NO is released from the proposed $[Cl_3Fe(\kappa^1\text{-S-Ph}_3CSNO)]^-$ adduct, then recaptured by $[Cl_6Fe^{II}_2]^2$ – generated from the decomposition of $[Cl_3Fe^{III}\text{-SCPh}_3]^-$. The key difference between

these two mechanisms is the identity of the brown intermediate prior to the formation of $[\text{Cl}_3\text{FeNO}]^-$ (highlighted in gray, Scheme 5). In Mechanism A, the brown intermediate should be $[\text{Cl}_3\text{Fe}(\kappa^1\text{-N-Ph}_3\text{CSNO})]^-$, whereas, for Mechanism B, it should be either $[\text{Cl}_3\text{Fe}(\kappa^1\text{-S-Ph}_3\text{CSNO})]^-$ or $[\text{Cl}_3\text{Fe}^{\text{III}}\text{-SCPh}_3]^-$. Characterization of the Fe^{III} Halothiolate Intermediate of the second second

Characterization of the Fe^{III} Halothiolate Intermediate. To further discern the two proposed mechanisms, we set out to identify the initial brown intermediate that absorbs at 520 and 630 nm. On the basis of Mechanism B, the brown intermediate could be $[Cl_3Fe(\kappa^1-S-Ph_3CSNO)]^-$, or if NO^o release has already occurred, the iron(III)—halothiolate $[Cl_3Fe^{III}-SCPh_3]^-$. We began our studies by first attempting to generate $[Cl_3Fe^{III}-SCPh_3]^-$ from an independent reaction between TBA $[Cl_4Fe^{III}]$ and NaSCPh₃. As shown in Figure 2,

$$[CI_4Fe^{|II}]^- \xrightarrow{NaSCPh_3} - NaCI \xrightarrow{Fe^{|II}} Fe^{|II} Fe^{|II} CI_{4-x}(SR)_x J^- impurities$$

$$0.6 - CI_{1}^{-1} CI_{2}^{-1} CI_{3}^{-1} Fe^{|II} (SCPh_3)_{3}^{-1} - [CI_4Fe^{|II}]^- + NaSCPh_3$$

$$0.2 - CI_3Fe^{|II}(SCPh_3)_{3}^{-1} - [CI_4Fe^{|II}]^- + NaSCPh_3$$

$$0.3 - CI_3Fe^{|II}(SCPh_3)_{3}^{-1} - [CI_4Fe^{|II}]^- + NaSCPh_3$$

$$0.4 - CI_3Fe^{|II}(SCPh_3)_{3}^{-1} - [CI_4Fe^{|II}]_{3}^{-1} + NaSCPh_3$$

Figure 2. Comparison of initial UV–vis spectra resulting from the reaction between $[Fe_2Cl_6]^{2-}$ and Ph_3CSNO at -50 °C in 1:1 THF/CH₃CN (0.5 mM, brown trace); the reaction between TBA[Cl_4Fe^{III}] and 1 equiv of NaSCPh₃ at -20 °C (0.5 mM, red trace).

the in situ UV–vis spectrum of the reaction of $TBA[Cl_4Fe^{III}]$ with 1 equiv of $NaSCPh_3$ in CH_3CN/THF (red trace) shows a good match with the brown intermediate. Further, the reaction between $FeCl_3$ and $TBA(SCPh_3)$ leads to the formation of the same spectrum, albeit at a lower spectroscopic yield (Figure S11). In addition, the predicted UV–vis spectrum of $[Cl_3Fe^{III}-SCPh_3]^-$ by time-dependent density functional theory (TD-DFT) at the TPSSh/def2-TZVP level correlates well with the experimental data (Figure S30). Additional independent experiments examining the reaction between $[Cl_6Fe^{II}_2]^{2-}$ and varying equivalents of $NaSCPh_3$ (Figure S12) also excluded the possibility of an Fe^{II} thiolate species being the identity of the brown intermediate.

Analysis of the brown intermediate with Mössbauer spectroscopy further supports its assignment as an Fe^{III} thiolate species. Independent generation of $[\text{Cl}_3^{57}\text{Fe}^{\text{III}}(\text{SCPh}_3)]^-$ from the reaction between TBA $[\text{Cl}_4^{57}\text{Fe}^{\text{III}}]$ and 1 equiv of NaSCPh₃ displays a Mössbauer spectrum similar to that produced from the reaction between TBA $_2[\text{Cl}_6^{57}\text{Fe}^{\text{II}}_2]$ and 2 equiv of Ph $_3$ CSNO (See Supporting Information, Figures S19, S20). Both spectra display peaks corresponding to two major species—the first one (ca. 40%) exhibiting isomer shift and quadrupole splitting values identical to that of TBA $_2[\text{Cl}_6^{-57}\text{Fe}^{\text{II}}_2]$ (δ = 1.16 mm s $^{-1}$, | ΔE_O | = 2.86 mm s $^{-1}$ (Figure S16)).

The second component (ca. 60%) displays an isomer shift of δ = 0.38 mm s⁻¹ and quadrupole splitting value of $|\Delta E_{\rm Q}|$ = 0.94 mm s⁻¹, which was assigned as $[{\rm Cl_3Fe^{III}(SCPh_3)}]^-$. These parameters are different from those of TBA $[{\rm Cl_4}^{57}{\rm Fe^{III}}]$ (Figure S18), which has an isomer shift value of δ = 0.23 mm s⁻¹ and a quadrupole splitting of $|\Delta E_{\rm Q}|$ = 0.53 mm s⁻¹ (Table 1).

Table 1. Solution Mössbauer Parameters

complex (major component)	$\delta \; (\text{mm/s})$	$\Delta E_{\rm Q} ({\rm mm/s})$
$TBA_2[Cl_6^{57}Fe_2^{II}]$	1.16	2.86
$TBA[Cl_4^{57}Fe^{III}]$	0.23	0.53
$TBA[Cl_4^{57}Fe^{III}] + NaSCPh_3$	0.38	0.94
TBA2[Cl657FeII2] + 2 Ph3CSNO	0.38	0.93

Despite our UV—vis and Mössbauer experiments providing spectroscopic evidence for the assignment of the brown intermediate as an Fe^{III} thiolate species, we were unable to obtain structural data on the putative $[Cl_3Fe^{III}\text{-SCPh}_3]^-$. Our inability to structurally characterize $[Cl_3Fe^{III}\text{-SCPh}_3]^-$ could be due to (1) the decomposition of $[Cl_3Fe^{III}\text{-SCPh}_3]^-$ to Ph₃CS-SCPh₃ and $[Cl_6Fe^{II}_2]^{2-}$ (see Supporting Information) or (2) the labile nature of the chloride ligands leading to complicated ligand scrambling that can generate other $[Cl_xFe^{III}$ -(SCPh₃)_{4-x}]⁻ (x = 1, 2, 3, 4). Indeed, titration experiments of NaSCPh₃ into TBA[Cl_4Fe^{III}], and TBA(SCPh₃) into FeCl₃ at -40 °C show formation of distinctly different species as additional amounts (1–5 equiv) of thiolate are added to Fe^{III} (Figures S13, S14). Nonetheless, with a 3:1:1 stoichiometry of Cl^- :Fe^{III}:Ph₃CS⁻, we believe the major iron(III) halothiolate species in solution at the low temperatures at which our studies were conducted is $[Cl_3Fe^{III}\text{-SCPh}_3]^-$.

In Situ IR Study of the Conversion of $[Cl_6Fe^{II}_2]^{2-}$ to $[Cl_3FeNO]^-$ by Ph₃CSNO. The in situ UV-vis and Mössbauer data so far suggest that reaction of $[Cl_6Fe^{II}_2]^{2-}$ with Ph₃CSNO first leads to the formation of an iron(III) halothiolate and free NO $^{\bullet}$. The iron(III) halothiolate then slowly decomposes to disulfide and $[Cl_6Fe^{II}_2]^{2-}$, which

captures free NO to form the [Cl₃FeNO] complex (Scheme 5, Mechanism B). Further support of Mechanism B was provided by an in situ time-resolved solution IR study. Addition of $[Cl_6Fe^{II}_2]^{2-}$ to a solution with 2 equiv of Ph₃CSNO in THF- d_8 at -70 °C results in a decrease of the peak at 1493 cm⁻¹ corresponding to Ph₃CSNO. Upon further warming of the reaction mixture to -50 °C, a new band at 1792 cm⁻¹ appeared, which was attributed to TBA[Cl₃FeNO] (Figure 3, left). 39 An 15N-labeling experiment confirmed that Ph₃CSNO and [Cl₃FeNO] were the only species observed with ¹⁵N-sensitive stretches over the course of the reaction (see SI, Figures S24, S25). Importantly, the initial decay of Ph₃CSNO was not accompanied by the formation of [Cl₃FeNO] (Figure 3, right). The 15 s time intervals at which the IR spectra were monitored allowed the time gap (ca. 90 s, see SI, Figures S22, S23) between these two events to be determined. The delay in [Cl₃FeNO]⁻ formation provides further assent that free NO was first released into the headspace, where it was unobservable by solution IR until it was recaptured by [Cl₆Fe^{II}₂]²⁻ as [Cl₃FeNO]⁻, consistent with Mechanism B (Scheme 5, bottom). These results are also in agreement with our UV-vis studies, where the formation of [Cl₃FeNO] was observed concurrently with the slow decay of the brown intermediate.

In situ UV—vis, Mössbauer, and IR spectroscopic studies allow us to conclude that NO $^{\bullet}$ release likely proceeds through coordination of the S atom to Fe^{II} prior to S—N bond cleavage. Otherwise, the concurrent formation of [Cl₃FeNO] $^{-}$ and consumption of Ph₃CSNO would be expected. The proposed mechanism is also consistent with the reactivity profile of metal S-nitrosothiol complexes— κ^{I} -S coordination weakens the S—N bond, making the release of NO $^{\bullet}$ more favorable (Scheme 3). ¹³

RSNO Formation from Putative Iron(III) Halothiolate.

As many NO[•] release/storage mechanisms are reversible in Nature,⁸ we next investigated whether the Fe^{II}/Fe^{III} chloride couple can carry out the formation of S-nitrosothiol. Lancaster et al. proposed that the LIP can promote RS–NO bond

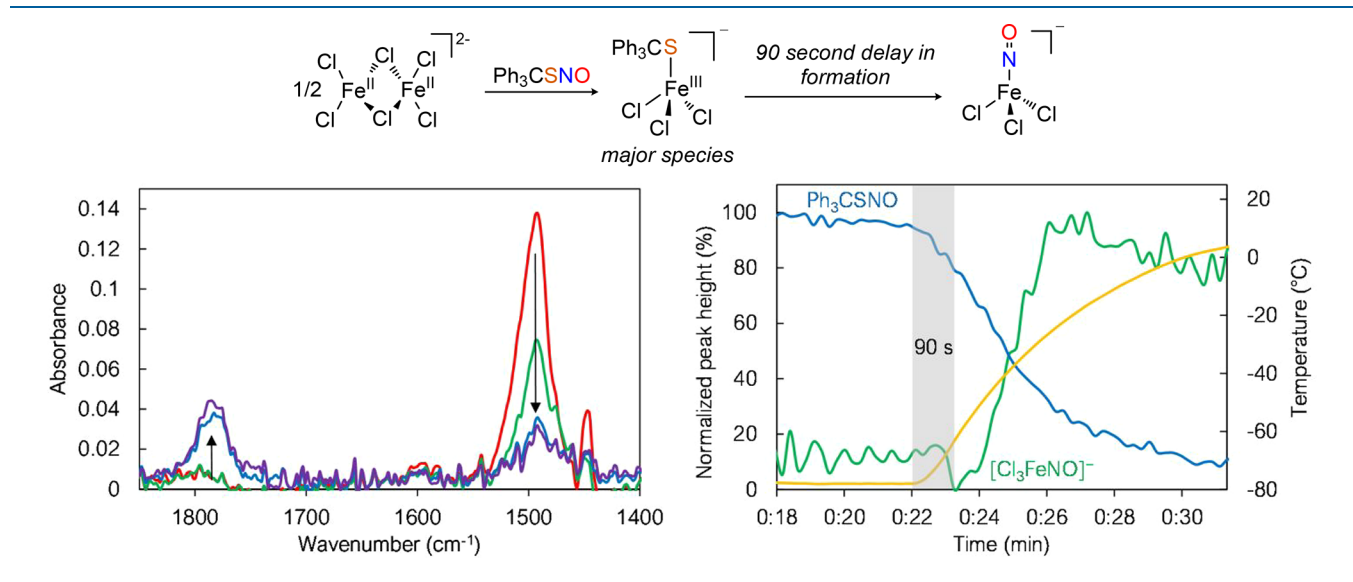


Figure 3. Left: Selected in situ solution IR spectra of the reaction between $[Fe_2Cl_6]^{2-}$ and Ph_3CSNO in THF- d_8 , 30 mM (from red to purple traces), showing the decrease in $\nu(NO) = 1493$ cm⁻¹ (Ph_3CSNO) and the appearance of $\nu(NO) = 1792$ cm⁻¹ ($[Cl_3FeNO]^-$) upon warming. Right: Normalized peak heights of Ph_3CSNO (blue) and $TBA[Cl_3FeNO]$ (green) versus time and temperature (yellow) shows a 90 s delay (shaded gray) in $TBA[Cl_3FeNO]$ formation.

formation based on the observation that the cellular protein S-nitrosation levels strongly depend on the concentration of labile/chelatable iron. 10,11 To this end, we first generated the putative $[Cl_3Fe^{III}SCPh_3]^-$ by treating $Fe^{III}Cl_3$ with TBA-(SCPh₃) at -78 °C and subjected this reaction mixture to sequential additions of NO $^{\bullet}$. In situ solution IR spectroscopy was utilized to monitor and quantify product formation. After the addition of 2 equiv of NO $^{\bullet}$ at -78 °C and upon warming the reaction mixture to -50 °C, we observed concurrent formation of peaks at 1792 and 1493 cm $^{-1}$ (Figure 4), assigned

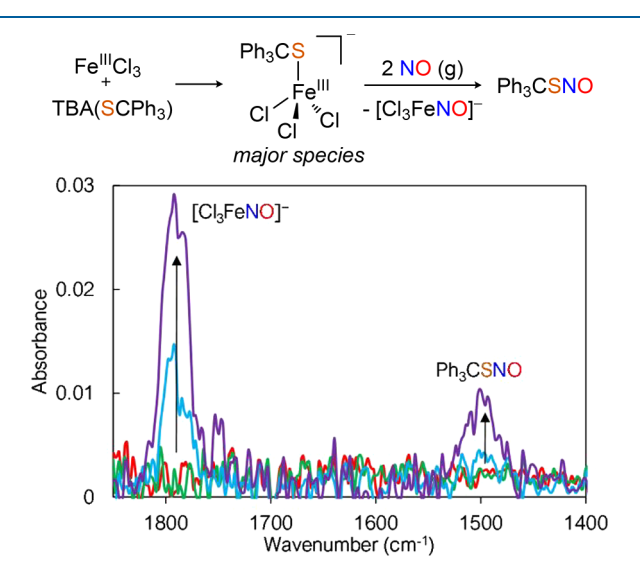
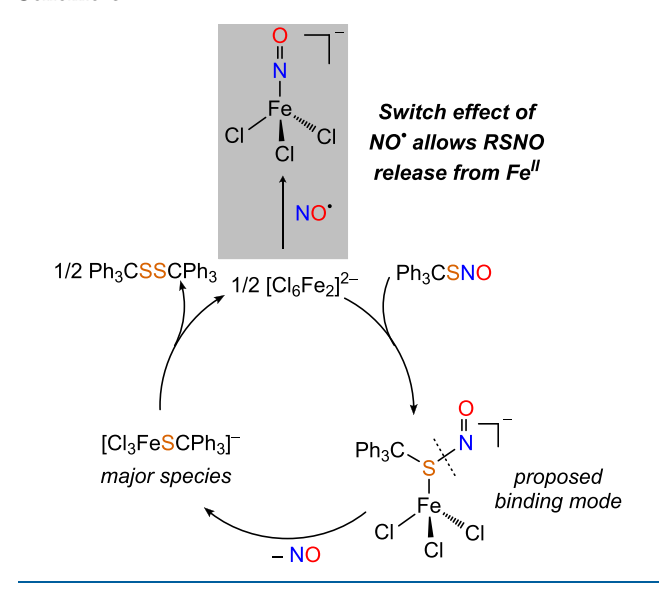


Figure 4. Selected in situ IR spectra of the reaction between $[Cl_3Fe^{III}SCPh_3]^-$ and 2 equiv of NO^{\bullet} in 9:1 THF- d_8/CD_3CN at -80 °C (30 mM). At -50 °C, formation of Ph_3CSNO ($\nu(NO)=1493$ cm $^{-1}$) and TBA[Cl_3FeNO] ($\nu(NO)=1792$ cm $^{-1}$) was observed.

as [Cl₃FeNO] and Ph₃CSNO, respectively. 39,45 The estimated yields of [Cl₃FeNO]⁻ and Ph₃CSNO were 67% and 50%, respectively, based on the IR absorbances (see Supporting Information, Figures S24, S25). The Fe^{III} center facilitates the oxidative coupling of thiolate and NO to form Ph₃CSNO by acting as an electron acceptor and undergoing reduction to Fe^{II}, which may be trapped by additional NO• to form [Cl₃FeNO]⁻. The presence of an additional equivalent of NO is critical to prevent the reverse reaction, that is, the release of NO[•] from Ph₃CSNO, as Fe^{II} complexes are known to lead to the decomposition of RSNO to disulfide and NO. (Scheme 6). The robust Fe-NO interaction impedes the displacement of the NO ligand by S-nitrosothiol and prevents the catalytic decomposition of RSNO (Scheme 6). Such a "switch effect" of NO epresents a key difference between Fe and Cu mediated S-nitrosothiol formation; the strong interaction between high-spin Fe^{III} (S = 5/2) with NO⁻ (S = 1) is not shared by Cu. In fact, some of us, and Hayton et al., have shown that the interaction of Cu^{II} and NO• is highly reversible.46,47

To confirm that $[\text{Cl}_3\text{FeNO}]^-$ does not participate in RS–NO bond formation, we investigated its reaction with thiolate (Scheme 7). Treatment of PPN[Cl $_3$ FeNO] with sodium *tert*-butyl thiolate affords a red-colored solution with strong absorbances at 360 nm ($\varepsilon = 6670 \text{ M}^{-1} \text{ cm}^{-1}$) and 475 nm ($\varepsilon = 4360 \text{ M}^{-1} \text{ cm}^{-1}$), which were assigned as PPN-[($^t\text{BuS})_3$ FeNO]. Titration of *tert*-butyl thiolate to a solution of PPN[Cl $_3$ FeNO] in the UV–vis spectrometer confirmed the

Scheme 6



Scheme 7

3:1 stoichiometry (Figure S6). While the titration of NaSCPh₃ to PPN[Cl₃FeNO] displays similar UV–vis spectra (Figure S7), employing *tert*-butyl thiolate allowed us to calculate the yield of the product [([†]BuS)₃FeNO]⁻ based on reported molar extinction coefficients. The spectroscopic yield of [([†]BuS)₃FeNO]⁻ was determined to be 99%, indicating that the {FeNO}⁷ motif is robust, while the Cl⁻ ligand exchange occurs with [†]BuS^{-,36}

Electronic Structure of [Cl₃FeNO]⁻, [Cl₃CuNO]⁻, and Cl₃FeNO. The inertness of [Cl₃FeNO] toward nitrosation of thiolate and the irreversible binding of NO^o at [Cl₃Fe^{II}] are a crucial part of Mechanism B proposed in Scheme 5. These properties of [Cl₂FeNO]⁻ are in sharp contrast to its Cu analogue [Cl₃CuNO]⁻, which exhibits both reversible binding with NO and nitrosative reactivity toward thiolates. To gain more insight into the different reactivities of [Cl₂FeNO] and [Cl₃CuNO]⁻, we utilized complete active space self-consistent field (CASSCF) computations to further understand their electronic structure (Figure 5). Some of us⁴⁶ and others^{39,46,48,49} have shown that CASSCF calculations can provide a detailed understanding of the correlation of electronic structure and reactivity of metal-nitrosyls. The state-specific CASSCF calculations were performed in each complex's well-established spin state, S = 3/2 for $[Cl_3FeNO]^-$ and S = 0 for $[Cl_3CuNO]^-$. After screening various combinations of metal 3d, NO- σ^* , and NO- π^* orbitals, we chose an active space of [9e,13o] for [Cl₃FeNO]⁻ and [10e,13o] for [Cl₃CuNO]⁻. These active spaces include (i) bonding and antibonding orbitals of NO- π^* with metal-d_{xz/yz} (ii) bonding and antibonding orbitals of NO- σ^* with metal- d_z^2 , (iii) nonbonding $d_{x^2-y^2/xy}$ as well as (iv) the next five unoccupied orbitals lowest in energy, which are often based on metal 4d or ancillary ligands Cl (see Supporting Information). We found that 4d orbitals and ancillary orbitals

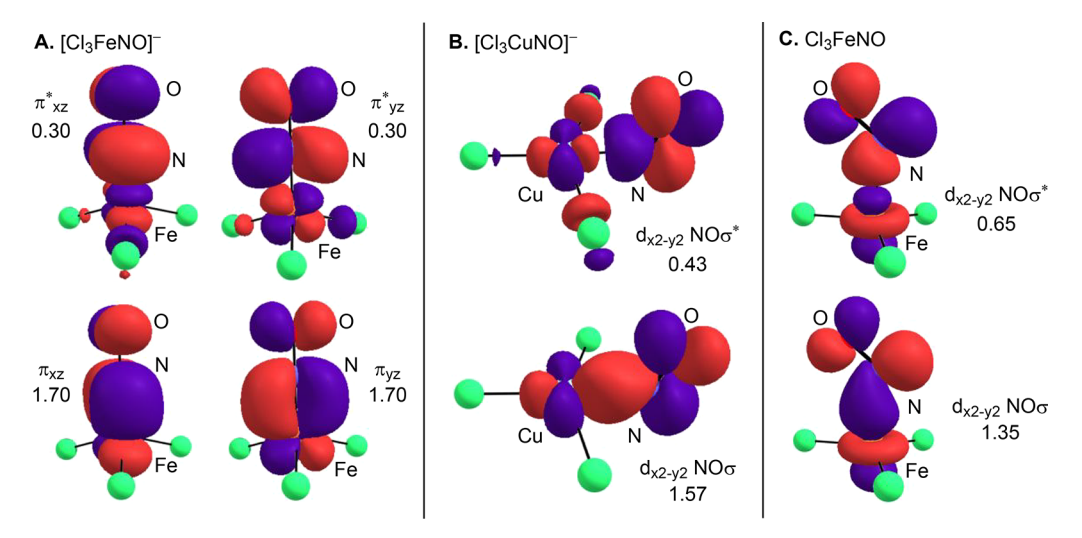


Figure 5. Partially occupied, covalent metal—NO frontier orbitals resulting from CASSCF calculations of the electronic ground states of (A) [Cl₃FeNO]⁻ [9e,13o], (B) [Cl₃CuNO]⁻ [10e,13o], and (C) Cl₃FeNO [6e, 13o].

have little effect on the results of the calculations, consistent with previous studies by Klüfers. To computationally estimate the amount of $NO^{-/\bullet/+}$ character in each complex, a valence bond-like interpretation of the CAS wave function was applied by following the method laid out by Radón et al. The amount of $NO^{-/\bullet/+}$ character in each species is summarized in Table 2. Intuitively, higher percentages of M^{n+1} - NO^+ character

Table 2. Results of Valence-Bond Analysis of Metal Nitrosyls

res. structure	[Cl ₃ FeNO] ⁻	[Cl ₃ CuNO] ⁻	Cl ₃ FeNO
M-NO-	52%	1%	0.25%
$M-NO^{\bullet}$	40%	86%	93%
M-NO ⁺	2%	10%	4%
others	5%	3%	2%

correlates to NO⁺ transfer (nitrosative) ability, while Mⁿ-NO[•] corresponds to free NO[•] release. We found the CASSCF results to be roughly consistent with the observed reactivity of [Cl₃FeNO]⁻ and [Cl₃CuNO]⁻. Specifically, [Cl₃FeNO]⁻ exhibits the lowest NO[•] character (38%) and NO⁺ character (2%), consistent with its inability to release free NO[•] and perform S-nitrosation. [Cl₃CuNO]⁻ exhibits significant NO[•] and NO⁺ character (86% and 10%, respectively) and is capable of both NO[•] release and S-nitrosation.

We were curious as to whether this qualitative analysis would allow us to predict the NO+ reactivity of Cl₃FeNO, the product of the one-electron oxidation of [Cl₃FeNO]⁻. This theoretical interaction of Fe^{III}Cl₃ with NO• would result in an $\{FeNO\}^6$ complex with a spin (S=2), which would be more likely to exhibit NO+ transferring ability. The geometry of putative Cl₃FeNO complex was optimized with DFT in a variety of spin states (S = 0, 1, 2). The two known non-heme {FeNO}⁶ complexes both have an experimentally and computationally determined S = 1 (Fe^{IV}-NO⁻) ground state; 52 however, optimization by B3LYP/def2-TZVP determined the S = 2 state in Cl_3FeNO to be the lowest in energy by -20.3 kcal/mol. CASSCF calculation on the S=2 spin state showed highly covalent bonding character between the Fe d_z^2 and NO p_x orbitals with 1.35 e⁻ in the bonding orbital and 0.65 e in the antibonding orbital (Figure 5C), similar to

[Cl₃CuNO]^{-.46} Post-localization recalculation of the CI coefficients shows Cl₃FeNO exhibits about 93% Fe^{III}-NO[•] character as the leading configuration, and Fe^{II}-NO⁺ contributes about 4.6% to the ground state as the second leading configuration. The increase in NO⁺ character in the Cl₃FeNO complex as compared to the [Cl₃FeNO]⁻ anion is consistent with our experimental observation that the Fe^{III} complex, but not Fe^{II}, is able to mediate an oxidative coupling reaction to form *S*-nitrosothiols.

SUMMARY AND CONCLUSIONS

In contrast to the RS $^{\bullet}$ expulsion mechanism from the κ^{1} -N RSNO species invoked during NO $^{\bullet}$ release from SNP, reaction of the high-spin $[Cl_{3}Fe^{II}]^{-}$ motif with S-nitrosothiol generates iron(III) thiolate and free NO $^{\bullet}$. Detailed in situ spectroscopic studies, including UV–vis, Mössbauer, and IR, suggest that coordination of the S atom to the iron(II) center is necessary to promote S–N bond cleavage. Importantly, iron(III) chloride complexes can also promote the formation of S-nitrosothiol when NO $^{\bullet}$ is in excess. Our CASSCF results, when paired alongside our experimental studies, highlight the possibility of the use of computation to predict the NO $^{-/{\bullet}/+}$ reactivity of a series of metal nitrosyl complexes.

One central question that remains unanswered within the literature is how Fe centers promote the storage of NO[•] as S-nitrosothiols, while also being efficient for the decomposition of RSNOs to NO[•] and disulfide. We believe the answer to this question lies within the ability of NO[•] to irreversibly bind to the Fe^{II} center ligated by weak field ligands, ^{34–37} shutting down coordination of S-nitrosothiol, which is a crucial step in its decomposition (Scheme 3). Since [Cl₃FeNO]⁻ can be easily converted to the DNIC [Cl₂Fe(NO)₂]⁻ in the presence of excess NO[•], ³⁹ our study also provides a potential explanation for the formation of DNIC and S-nitrosothiol frequently observed during cellular protein S-nitrosation ^{10,11} and demonstrates a strategy available to Nature to reversibly modulate biological NO[•] concentration with labile iron ions.

ASSOCIATED CONTENT

Solution Supporting Information

The Supporting Information is available free of charge at https://pubs.acs.org/doi/10.1021/acs.inorgchem.1c00203.

Experimental details, including characterization data, spectra, computational procedures, and results. Crystallographic data for $TBA_3[Cl_6Fe^{II}_2]\cdot[Cl_3Fe^{II}(H_2O)]$ (CSD: 2057290) (PDF)

Accession Codes

CCDC 2057290 contains the supplementary crystallographic data for this paper. These data can be obtained free of charge via www.ccdc.cam.ac.uk/data_request/cif, or by emailing data_request@ccdc.cam.ac.uk, or by contacting The Cambridge Crystallographic Data Centre, 12 Union Road, Cambridge CB2 1EZ, UK; fax: +44 1223 336033.

AUTHOR INFORMATION

Corresponding Author

Shiyu Zhang — Department of Chemistry & Biochemistry, The Ohio State University, Columbus, Ohio 43210, United States; orcid.org/0000-0002-2536-4324; Email: zhang.8941@osu.edu

Author

Anna L. Poptic – Department of Chemistry & Biochemistry, The Ohio State University, Columbus, Ohio 43210, United States

Complete contact information is available at: https://pubs.acs.org/10.1021/acs.inorgchem.1c00203

Notes

The authors declare no competing financial interest.

ACKNOWLEDGMENTS

We acknowledge the Ohio Supercomputer Center for highperformance computing resources, and Prof. Alexander Sokolov for help with CASSCF calculations. This publication is based on work funded by the National Science Foundation under award no. CHE-1904560. The authors thank The Ohio State University Department of Chemistry and Biochemistry for additional financial support.

REFERENCES

- (1) Ignarro, L. J. Nitric Oxide: Biology and Pathobiology; Elsevier: Amsterdam, 2009.
- (2) Rassaf, T.; Kleinbongard, P.; Preik, M.; Dejam, A.; Gharini, P.; Lauer, T.; Erckenbrecht, J.; Duschin, A.; Schulz, R.; Heusch, G.; Feelisch, M.; Kelm, M. Plasma Nitrosothiols Contribute to the Systemic Vasodilator Effects of Intravenously Applied NO: Experimental and Clinical Study on the Fate of NO in Human Blood. *Circ. Res.* 2002, 91, 470–477.
- (3) Broniowska, K. A.; Hogg, N. The Chemical Biology of S-Nitrosothiols. *Antioxid. Redox Signaling* **2012**, *17*, 969–980.
- (4) Hess, D. T.; Matsumoto, A.; Kim, S. O.; Marshall, H. E.; Stamler, J. S. Protein S-Nitrosylation: Purview and Parameters. *Nat. Rev. Mol. Cell. Biol.* **2005**, *6*, 150–166.
- (5) Anand, P.; Stamler, J. S. Enzymatic Mechanisms Regulating Protein S-Nitrosylation: Implications in Health and Disease. *J. Mol. Med.* **2012**, *90*, 233–244.
- (6) Melzer, M. M.; Mossin, S.; Cardenas, A. J. P.; Williams, K. D.; Zhang, S.; Meyer, K.; Warren, T. H. A Copper(II) Thiolate from Reductive Cleavage of an S-Nitrosothiol. *Inorg. Chem.* **2012**, *51*, 8658–8660.
- (7) Zhang, S.; Çelebi-Ölçüm, N.; Melzer, M. M.; Houk, K. N.; Warren, T. H. Copper(I) Nitrosyls from Reaction of Copper(II) Thiolates with S-Nitrosothiols: Mechanism of NO Release from RSNOs at Cu. J. Am. Chem. Soc. 2013, 135, 16746–16749.

- (8) Zhang, S.; Melzer, M. M.; Sen, S. N.; Çelebi-Ölçüm, N.; Warren, T. H. A Motif for Reversible Nitric Oxide Interactions in Metalloenzymes. *Nat. Chem.* **2016**, *8*, 663–669.
- (9) Zhang, C.; Biggs, T. D.; Devarie-Baez, N. O.; Shuang, S.; Dong, C.; Xian, M. S-Nitrosothiols: Chemistry and Reactions. *Chem. Commun.* **2017**, *53*, 11266–11277.
- (10) Li, Q.; Li, C.; Mahtani, H. K.; Du, J.; Patel, A. R.; Lancaster, J. R. Nitrosothiol Formation and Protection against Fenton Chemistry by Nitric Oxide-Induced Dinitrosyliron Complex Formation from Anoxia-Initiated Cellular Chelatable Iron Increase. *J. Biol. Chem.* **2014**, 289, 19917–19927.
- (11) Bosworth, C. A.; Toledo, J. C.; Zmijewski, J. W.; Li, Q.; Lancaster, J. R. Dinitrosyliron Complexes and the Mechanism(s) of Cellular Protein Nitrosothiol Formation from Nitric Oxide. *Proc. Natl. Acad. Sci. U. S. A.* **2009**, *106*, 4671–4676.
- (12) Hottinger, D. G.; Beebe, D. S.; Kozhimannil, T.; Prielipp, R. C.; Belani, K. G. Sodium Nitroprusside in 2014: A Clinical Concepts Review. *J. Anaesthesiol. Clin. Pharmacol.* **2014**, *30*, 462–471.
- (13) Rhine, M. A.; Sanders, B. C.; Patra, A. K.; Harrop, T. C. Overview and New Insights into the Thiol Reactivity of Coordinated NO in $\{MNO\}^{6/7/8}$ (M = Fe, Co) Complexes. *Inorg. Chem.* **2015**, *54*, 9351–9366.
- (14) Hunt, A. P.; Lehnert, N. The Thiolate Trans Effect in Heme {FeNO}⁶ Complexes and Beyond: Insight into the Nature of the Push Effect. *Inorg. Chem.* **2019**, *58*, 11317–11332.
- (15) Goodrich, L. E. Model Complexes of Cytochrome P450 Nitric Oxide Reductase. Ph.D. Thesis, The University of Michigan, Ann Arbor, MI, 2012.
- (16) Weichsel, A.; Maes, E. M.; Andersen, J. F.; Valenzuela, J. G.; Shokhireva, T. K.; Walker, F. A.; Montfort, W. R. Heme-Assisted S-Nitrosation of a Proximal Thiolate in a Nitric Oxide Transport Protein. *Proc. Natl. Acad. Sci. U. S. A.* **2005**, 102, 594–599.
- (17) Basu, S.; Keszler, A.; Azarova, N. A.; Nwanze, N.; Perlegas, A.; Shiva, S.; Broniowska, K. A.; Hogg, N.; Kim-Shapiro, D. B. A Novel Role for Cytochrome c: Efficient Catalysis of S-Nitrosothiol Formation. *Free Radical Biol. Med.* **2010**, *48*, 255–263.
- (18) Franke, A.; Stochel, G.; Suzuki, N.; Higuchi, T.; Okuzono, K.; Van Eldik, R. Mechanistic Studies on the Binding of Nitric Oxide to a Synthetic Heme-Thiolate Complex Relevant to Cytochrome P450. *J. Am. Chem. Soc.* **2005**, *127*, 5360–5375.
- (19) Gao, Y.; Mossing, B.; Wu, G. Direct NMR Detection of the Unstable "Red Product" from the Reaction between Nitroprusside and 2-Mercaptosuccinic Acid. *Dalt. Trans.* **2015**, *44*, 20338–20343.
- (20) Schwane, J. D.; Ashby, M. T. FTIR Investigation of the Intermediates Formed in the Reaction of Nitroprusside and Thiolates. *J. Am. Chem. Soc.* **2002**, *124*, 6822–6823.
- (21) Perissinotti, L. L.; Estrin, D. A.; Leitus, G.; Doctorovich, F. A Surprisingly Stable S-Nitrosothiol Complex. J. Am. Chem. Soc. 2006, 128, 2512–2513.
- (22) Hosseininasab, V.; McQuilken, A. C.; Bakhoda, A.; Bertke, J. A.; Timerghazin, Q. K.; Warren, T. H. Lewis Acid Coordination Redirects S-Nitrosothiol Signaling Output. *Angew. Chem.* **2020**, *132*, 10946–10950.
- (23) Timerghazin, Q. K.; Peslherbe, G. H.; English, A. M. Resonance Description of S-Nitrosothiols: Insights into Reactivity. *Org. Lett.* **2007**, *9*, 3049–3052.
- (24) Hendinejad, N.; Timerghazin, Q. K. Biological Control of: S-Nitrosothiol Reactivity: Potential Role of Sigma-Hole Interactions. *Phys. Chem. Phys.* **2020**, 22, 6595–6605.
- (25) Roncaroli, F.; Van Eldik, R.; Olabe, J. A. Release of NO from Reduced Nitroprusside Ion. Iron-Dinitrosyl Formation and NO-Disproportionation Reactions. *Inorg. Chem.* **2005**, *44*, 2781–2790.
- (26) Petrat, F.; de Groot, H.; Sustmann, R.; Rauen, U. The Chelatable Iron Pool in Living Cells: A Methodically Defined Ouantity. *Biol. Chem.* **2002**, *383*, 489–502.
- (27) Lok, H. C.; Sahni, S.; Jansson, P. J.; Kovacevic, Z.; Hawkins, C. L.; Richardson, D. R. A Nitric Oxide Storage and Transport System That Protects Activated Macrophages from Endogenous Nitric Oxide Cytotoxicity. *J. Biol. Chem.* **2016**, 291, 27042–27061.

- (28) Damasceno, F. C.; Condeles, A. L.; Lopes, A. K. B.; Facci, R. R.; Linares, E.; Truzzi, D. R.; Augusto, O.; Toledo, J. C. The Labile Iron Pool Attenuates Peroxynitrite-Dependent Damage and Can No Longer Be Considered Solely a pro-Oxidative Cellular Iron Source. *J. Biol. Chem.* **2018**, *293*, 8530–8542.
- (29) Kruszewski, M. Labile Iron Pool: The Main Determinant of Cellular Response to Oxidative Stress. *Mutat. Res., Fundam. Mol. Mech. Mutagen.* **2003**, 531, 81–92.
- (30) Fitzpatrick, J.; Kim, E. Synthetic Modeling Chemistry of Iron-Sulfur Clusters in Nitric Oxide Signaling. *Acc. Chem. Res.* **2015**, 48, 2453–2461.
- (31) Tran, C. T.; Kim, E. Acid-Dependent Degradation of a [2Fe-2S] Cluster by Nitric Oxide. *Inorg. Chem.* **2012**, *51*, 10086–10088.
- (32) Crack, J. C.; Smith, L. J.; Stapleton, M. R.; Peck, J.; Watmough, N. J.; Buttner, M. J.; Buxton, R. S.; Green, J.; Oganesyan, V. S.; Thomson, A. J.; Le Brun, N. E. Mechanistic Insight into the Nitrosylation of the [4Fe-4S] Cluster of WhiB-like Proteins. J. Am. Chem. Soc. 2011, 133, 1112–1121.
- (33) Harrop, T. C.; Tonzetich, Z. J.; Reisner, E.; Lippard, S. J. Reactions of Synthetic [2Fe-2S] and [4Fe-4S] Clusters with Nitric Oxide and Nitrosothiols. *J. Am. Chem. Soc.* **2008**, *130*, 15602–15610.
- (34) McQuilken, A. C.; Matsumura, H.; Dürr, M.; Confer, A. M.; Sheckelton, J. P.; Siegler, M. A.; McQueen, T. M.; Ivanović-Burmazović, I.; Moënne-Loccoz, P.; Goldberg, D. P. Photoinitiated Reactivity of a Thiolate-Ligated, Spin-Crossover Nonheme {FeNO}⁷ Complex with Dioxygen. *J. Am. Chem. Soc.* **2016**, *138*, 3107–3117.
- (35) Ting-Wah Chu, C.; Yip-Kwai Lo, F.; Dahl, L. F. Synthesis and Stereochemical Analysis of the $[Fe_4(NO)_4(\mu_3-S)_4]$ n Series (n=0,-1) Which Possesses a Cubanelike Fe_4S_4 Core: Direct Evidence for the Antibonding Tetrametal Character of the Un. *J. Am. Chem. Soc.* **1982**, 104, 3409–3422.
- (36) Harrop, T. C.; Song, D.; Lippard, S. J. Interaction of Nitric Oxide with Tetrathiolato Iron(II) Complexes: Relevance to the Reaction Pathways of Iron Nitrosyls in Sulfur-Rich Biological Coordination Environments. J. Am. Chem. Soc. 2006, 128, 3528–3529
- (37) Conradie, J.; Quarless, D. A.; Hsu, H. F.; Harrop, T. C.; Lippard, S. J.; Koch, S. A.; Ghosh, A. Electronic Structure and FeNO Conformation of Nonheme Iron-Thiolate-NO Complexes: An Experimental and DFT Study. *J. Am. Chem. Soc.* **2007**, *129*, 10446–10456.
- (38) Sun, J. S.; Zhao, H.; Ouyang, X.; Clérac, R.; Smith, J. A.; Clemente-Juan, J. M.; Gómez-Garcia, C.; Coronado, E.; Dunbar, K. R. Structures, Magnetic Properties, and Reactivity Studies of Salts Containing the Dinuclear Anion $[M_2Cl_6]^{2-}$ (M = Mn, Fe, Co). *Inorg. Chem.* 1999, 38, 5841–5855.
- (39) In-Iam, A.; Wolf, M.; Wilfer, C.; Schaniel, D.; Woike, T.; Klüfers, P. {FeNO}⁷-Type Halogenido Nitrosyl Ferrates: Syntheses, Bonding, and Photoinduced Linkage Isomerism. *Chem. Eur. J.* **2019**, 25, 1304–1325.
- (40) Kohlschütter, V.; Sazanoff, P. Zur Kenntnis Der Metallnitrosoverbindungen. Ber. Dtsch. Chem. Ges. 1911, 44, 1423–1432.
- (41) Begel, S.; Puchta, R.; Sutter, J.; Heinemann, F. W.; Dahlenburg, L.; van Eldik, R. Studies on the Reaction of Iron(II) with NO in a Noncoordinating Ionic Liquid. *Inorg. Chem.* **2015**, *54*, 6763–6775.
- (42) Steimann, M.; Nagel, U.; Grenz, R.; Beck, W. Die Struktur von Trichloronitrosylferrat, [Fe(NO)Cl₃]. *J. Organomet. Chem.* **1983**, 247. 171–174.
- (43) Ivanova, L. V.; Cibich, D.; Deye, G.; Talipov, M. R.; Timerghazin, Q. K. Modeling of S-Nitrosothiol—Thiol Reactions of Biological Significance: HNO Production by S-Thiolation Requires a Proton Shuttle and Stabilization of Polar Intermediates. *ChemBio-Chem* **2017**, *18*, 726—738.
- (44) Khomyakov, D. G.; Timerghazin, Q. K. Toward Reliable Modeling of S-Nitrosothiol Chemistry: Structure and Properties of Methyl Thionitrite (CH₃SNO), an S-Nitrosocysteine Model. *J. Chem. Phys.* **2017**, *147*, 044305.

- (45) Melzer, M. M.; Jarchow-Choy, S.; Kogut, E.; Warren, T. H. Reductive Cleavage of O-, S-, and N-Organonitroso Compounds by Nickel(I) β -Diketiminates. *Inorg. Chem.* **2008**, 47, 10187–10189.
- (46) Bower, J. K.; Sokolov, A. Y.; Zhang, S. Four-Coordinate Copper Halonitrosyl {CuNO}¹⁰ Complexes. *Angew. Chem., Int. Ed.* **2019**, *58*, 10225–10229.
- (47) Wright, A. M.; Wu, G.; Hayton, T. W. Structural Characterization of a Copper Nitrosyl Complex with a {CuNO}¹⁰ Configuration. *J. Am. Chem. Soc.* **2010**, *132*, 14336–14337.
- (48) Tomson, N. C.; Crimmin, M. R.; Petrenko, T.; Rosebrugh, L. E.; Sproules, S.; Boyd, W. C.; Bergman, R. G.; DeBeer, S.; Toste, F. D.; Wieghardt, K. A Step beyond the Feltham-Enemark Notation: Spectroscopic and Correlated Ab Initio Computational Support for an Antiferromagnetically Coupled M(II)-(NO)⁻ Description of Tp*M-(NO) (M = Co, Ni). *J. Am. Chem. Soc.* **2011**, *133*, 18785–18801.
- (49) Monsch, G.; Klüfers, P. $[Fe(H_2O)_5(NO)]^{2+}$, the "Brown-Ring" Chromophore. *Angew. Chem., Int. Ed.* **2019**, 58, 8566–8571.
- (50) Griffith, W. P.; Lewis, J.; Wilkinson, G. Some Nitric Oxide Complexes of Iron and Copper. J. Chem. Soc. 1958, 3993–3998.
- (51) Radón, M.; Broclawik, E.; Pierloot, K. Electronic Structure of Selected {FeNO}⁷ Complexes in Heme and Non-Heme Architectures: A Density Functional and Multireference Ab Initio Study. *J. Phys. Chem. B* **2010**, *114*, 1518–1528.
- (52) Lehnert, N.; Fujisawa, K.; Camarena, S.; Dong, H. T.; White, C. J. Activation of Non-Heme Iron-Nitrosyl Complexes: Turning up the Heat. *ACS Catal.* **2019**, *9*, 10499–10518.